IJST, Transactions of Mechanical Engineering, Vol. 35, No. M2, pp 167-180
Printed in The Islamic Republic of Iran, 2011

MESHLESS ANALYSIS OF BACKWARD EXTRUSION BY NATURAL ELEMENT METHOD*

S.A.S. JAVANMARD[1**], F. DANESHMAND[2], M. M. MOSHKSAR[3] AND R. EBRAHIMI[4]

[1,2]Faculty of Mechanical Engineering, Shiraz University, Shiraz, I. R. of Iran
Email: ajavanmard@miau.ac.ir
[3,4]Dept. of Materials Science and Engineering, School of Engineering, Shiraz University, Shiraz, I. R. of Iran

Abstract– In this paper, a computational technique is presented based on the natural element method (NEM) for large plastic deformation simulation of the metal forming problems. NEM is a numerical technique in the field of computational mechanics and can be considered as a meshless method. The selected process is backward extrusion for circular shape hollow components from round billets. The punch stroke value is divided into sub-steps, whereas a new set of nodes become active at the end of each sub-step of deformation. Solutions are obtained for different area reductions under friction condition. Hollman-Ludwik law is selected to explain the material behavior after the yielding point. The experiments are carried out with fully annealed commercial aluminum alloy billets at room temperature, using various punch sizes. A set of die and punches are designed and constructed for experimental works. The validity of the proposed method is verified by comparing the results from deformed geometry, contours of equivalent strain and forming loads with those obtained from finite element simulation and experimental measurements. It is concluded that the results obtained by NEM are in good agreement with those from FEM and experiments and therefore, the meshless natural element method is capable of handling large plastic deformation.

Keywords– Metal forming, backward extrusion, natural element method, meshless methods, finite element method

1. INTRODUCTION

Extrusion (backward and forward) is one of the most utilized bulk metal forming processes. It is particularly suitable when high reductions in area are required. It is a difficult task to simulate a non-linear metal forming process involving large material deformation, history dependent material behavior and contact simulation. Using the finite element method (FEM) for simulation of metal forming processes originated in the late 1960s. Marcal and King [1] and McMeeking and Rice [2] used FEM for steady state metal forming simulation. Gouveia et al. [3] simulated cold forward extrusion by using updated Lagrangian and combined Eulerian-Lagrangian formulation and found excellent agreement for the flow pattern and strain distribution within the plastically deformed region. Moshksar and Ebrahimi [4, 5] used upper bound analysis in backward extrusion for circular and regular polygonal components and compared load stroke and material flow between upper bound theory and experimental results.

Although the finite element method is robust and has been thoroughly developed, it needs regeneration of the meshes in solving the metal forming problems. When the mesh becomes too distorted in a particular domain, a new mesh must be generated and the variables associated with material history must be mapped from the old mesh to the new. This introduces additional errors that meshless formulation can avoid. To overcome the difficulty associated with remeshing, the past decade has seen a tremendous

*Received by the editors March 2, 2011; Accepted September 19, 2011.
**Corresponding author

surge in the development of a family of Galerkin and collocation-based numerical methods known as particle, gridless, meshfree, or meshless methods. The meshless method is a node-based numerical method and has various ways to solve the metal forming problems. Some essential advantages of the meshless methods are: a) The approximation functions are not dependent upon the meshes. This reduces the difficulties resulted from the distorted meshes. b) Only the nodal position information is needed. c) In the meshless methods, the results on the elements boundaries are smooth and continuous, whereas in FEM, there may be some discontinuity on the edge of the elements.

In metal forming simulation, Guo and Nakanishi [6] used element-free Galerkin (EFG) method with moving least squares approximation to simulate plane strain backward extrusion. Guan et al. [7] used element-free Galerkin method for non-steady metal forming processes simulation.

Liew et al. [8] used reproducing kernel particle for large deformation analysis in simply-supported beam under uniform pressure and etc., Lu et al. [9] simulate the buckling in sheet metal forming based on meshfree, Alfaro et al. [10] focus on the description and analysis of the NEM and its application for simulation of some forming processes involving large displacements. Li et al. [11] simulated ring upsetting based on corrected smooth particle hydrodynamics (SPH).

The natural element method (NEM) is a Galerkin-based method that is built upon the notion of natural neighbor interpolation. This interpolation scheme has very striking properties, such as its strictly interpolating character, ability to exactly interpolate piece-wise linear boundary conditions, and a well-defined and robust approximation with no user-defined parameter on non-uniform grids.

Non steady-state metal forming problems such as backward extrusion involve high mesh distortion with large material deformation and boundary motion, non-linear material behavior, and continuous changes in boundary conditions. In this paper, the authors' aim is to present the procedure developed on natural element and dividing punch stroke to sub-steps. First, the distribution of nodes in the probable solving domain is assumed and at the end of each sub-step, active nodes are selected for next step solution. These nodes constitute the new solving domain. The experiments are also designed in order to cover axisymmetric material flows commonly found in metal forming processes. Solutions are obtained for different area reductions under sliding friction condition. For the metal flow consideration, the workpieces are cut into halves before extrusion and a square grid printed onto the contacting surfaces in order to facilitate visualization of metal flow. Hook and Hollman-Ludwik laws are respectively used to explain material behavior in elastic and non-linear plastic parts. Remeshing process is used for FEM simulation [12]. A MATLAB code is established for the FEM and NEM simulation. The accuracy of the proposed method is verified by comparing the results for material flow, geometry, forming load and equivalent strain distributions with those obtained from experimental measurements and FEM results.

2. THE NATURAL ELEMENT METHOD

NEM is based on an interpolation plan called natural neighbor interpolation frequently used for unstructured interpolation in geophysics [13, 14]. This interpolation scheme is, in turn, based on the concepts of voronoi diagram and delaunay triangulations [15].

For a given problem domain with arbitrary geometry as shown in Fig. 1, a set of nodes are used to represent the internal domain and its boundary. Then, suppose that on sample point $\boldsymbol{X}$ is a random numerical integral point in the domain Ω (Fig. 2).

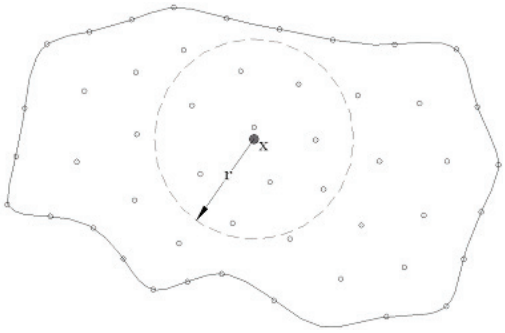

Fig. 1. Discrete node model in region Ω and the arbitrary integrate point

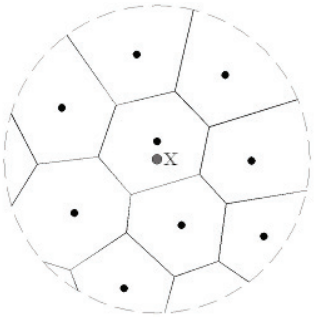

Fig. 2. Voronoi tessellation on nodes in assumed region

A Delaunay triangulation is the unique triangulation for a given set of points that satisfies the empty circumcircle. This means that the circumcircle of each triangle contains no other point than the three points that form the triangle. The Delaunay triangulation is the dual structure of the Voronoi tessellation (also known as Dirichlet tessellation). Each Voronoi cell represents the space closest to a given node. Thus, a first-order Voronoi diagram for a set of nodes $N=\{n_1,n_2,\ldots,n_m\} \in R^2$ is a subdivision of the space in regions T_I such that any point in T_I is closer to the node n_I, to which this region is associated, than to any other in N. Formally

$$T_I = \left\{x \in R^2 : d\left(x,n_I\right) < d\left(x,n_J\right) \quad \forall \quad J \neq I\right\} \tag{1}$$

where *d(.,.)* represents Euclidean distance. Two nodes whose associated Voronoi cells share an edge are called natural neighbors.

The Voronoi tessellation is always unique but the polygons associated with points on the boundary of the convex hull are unbounded. This has important consequences in the interpolation scheme, as will be demonstrated. A Voronoi polygon is thus the intersection of the half spaces defined by perpendicular bisecting lines to the segment joining each pair of nodes n_I, n_J.

The natural neighbor interpolation scheme is based on the definition of the second order Voronoi tessellation (Fig. 2). A cell T_{IJ} in the second-order tessellation is the locus of points that have node *I* as the closest node and the node J as the second closest node

$$T_{IJ} = \left\{x \in R^2 : d\left(x,n_I\right) < d\left(x,n_J\right) < d\left(x,n_K\right) \quad \forall \quad K \neq I,J\right\} \tag{2}$$

If a new point *x* is introduced in the initial set *N* and the new tessellation is built, the natural neighbor co-ordinates of the point *x* with respect to one of its neighbors *I* is defined as the ratio of the area of T_I that has been transferred to T_x to the total area of T_{xI}.

Sukumar et al. [15] presented this definition more formally. Using k(x) and $k_I(x)$ as Lebesgue measures (length in R^2) of T_x and T_{xI}, the natural neighbor co-ordinate of *x* with respect to the node *I* can be written as:

$$\varphi_I(x) = k_I(x)/k(x) \tag{3}$$

where, (Fig. 3)

$$\varphi_1 = A_{aef} \,/\, A_{abcde} \tag{4}$$

The other interpolation functions are presented in Table 1 and are compared with the interpolation functions obtained from FEM (Fig. 4).

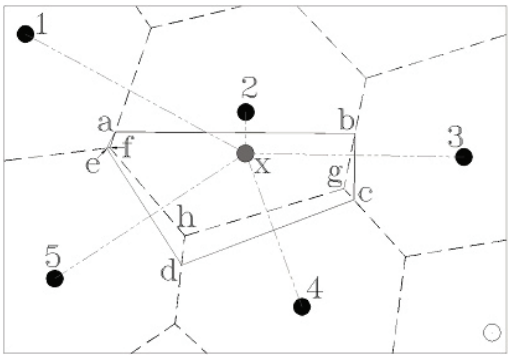

Fig. 3. Definition of the natural neighbor co-ordinates for determination interpolation functions of point x based on NEM

Table 1. Interpolation functions in FEM and NEM

Interpolation function	φ_1	φ_2	φ_3	φ_4	φ_5
FEM	0	A_{x45}/A_{245}	0	A_{x25}/A_{245}	A_{x24}/A_{245}
NEM	A_{aef}/A_{abcde}	A_{abghf}/A_{abcde}	A_{bcg}/A_{abcde}	A_{cdhg}/A_{abcde}	A_{defh}/A_{abcde}

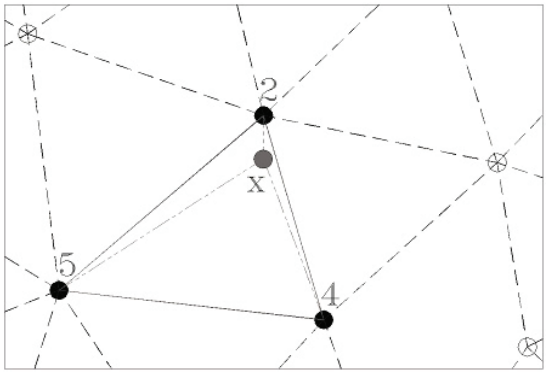

Fig. 4. Determination interpolation functions of point x based on FEM

From this definition, the unknown parameter field $u(x): \Omega \subset R^2 \rightarrow R^2$ is approximated in the form

$$u^h(x) = \sum_{I=1}^{n} \varphi_I(x) \;\; u_I \tag{5}$$

where u_I is the vector of nodal parameters of the n natural neighbors of the point x. NEM formulated in this way has some remarkable properties in the context of meshless methods [15].

Using Eq. (3) and Eq. (4), it is clear that

$$\varphi_i(x_j) = \delta_{ij} \tag{6}$$

and, consequently, the nodal parameters u_I are the nodal displacement. This allows us to impose nodal prescribed values by directly substituting them in the Galerkin procedure. It has also been proved that the NEM interpolation functions form a partition of unity [15].

The linear consistency of the interpolant is derived after the local co-ordinate property

$$x = \sum_{I=1}^{n} \varphi_I(x) x_J \tag{7}$$

in conjunction with the partition of unity property. This means that the natural neighbor interpolant can exactly reproduce a linear or constant displacement field. In the two-dimensional case, the approximation properties of the NEM interpolant depend on the relative node distribution. If a point x has only three natural neighbors, the interpolation obtained is equivalent to barycentric co-ordinates, or constant strain finite element interpolation functions. Bilinear interpolation is obtained over the rectangle if the point has four natural neighbors in a regular grid.

Another important property of natural neighbor interpolants is the ability to reproduce linear displacement fields over the boundary of convex domains [15].

3. NEM FORMULATION FOR LARGE PLASTIC DEFORMATION PROBLEMS

a) NEM matrices for large plastic deformation problems

The object of the mathematical theory of plasticity is to provide a theoretical description of the relationship between stress and strain for the material which exhibits an elasto-plastic response. In essence, plastic behavior is characterized by an irreversible straining which is not time dependent and can only be sustained once a certain level of stress has been reached. The yield criterion used is Von-Mises.

The discretized matrix equation, by applying the natural element shape function to the incremental governing equation is of the form [8]:

$$K\Delta u = \Delta F \tag{8}$$

where the stiffness matrix K is given as:

$$K = \int_{\Omega} B_I{}^T D B_J d\Omega \qquad \text{for the first iteration} \tag{9}$$

$$K = K_{NL} + K_G \qquad \text{for the other iteration} \tag{10}$$

with **D** being the elastic matrix, and

$$B_I{}^T = \begin{bmatrix} \partial\varphi_I/\partial X_1 & 0 & \partial\varphi_I/\partial X_2 & 0 \\ 0 & \partial\varphi_I/\partial X_2 & \partial\varphi_I/\partial X_1 & 0 \end{bmatrix} \tag{11}$$

$$K_{NL} = \int_{\Omega} B_{NLI}{}^T D_{ep} B_{NLJ} d\Omega \tag{12}$$

$$K_G = \int_{\Omega} B_{GI}{}^T Q B_{GJ} d\Omega \tag{13}$$

$$B_{NLI} = B_I F^T \tag{14}$$

$$B_{GI}{}^{T} = \begin{bmatrix} \partial\varphi_I/\partial X_1 & \partial\varphi_I/\partial X_2 & 0 & 0 \\ 0 & 0 & \partial\varphi_I/\partial X_1 & \partial\varphi_I/\partial X_2 \end{bmatrix} \tag{15}$$

F is the deformation gradient matrix and Q is the initial stress matrix. The elasto-plastic incremental stress-strain relation is defined by,

$$d\sigma = D_{ep} d\varepsilon \tag{16}$$

$$\left[D_{ep}\right] = \left[D\right] - \frac{\left[D\right]\left[a\right]\left[a\right]^T\left[D\right]}{H + \left[a\right]^T\left[D\right]\left[a\right]} \tag{17}$$

Based on Von-Mises yield criteria, the flow vector a is equal to,

$$\left[a\right]^T = \frac{\sqrt{3}}{2\sqrt{\tau_{xy}^2 + 0.5\left(\sigma_x'^2 + \sigma_y'^2 + \sigma_z'^2\right)}} \left\{\sigma_x' \quad \sigma_y' \quad 2\tau_{xy} \quad \sigma_z'\right\} \tag{18}$$

and H is the strain hardening coefficient defined by:

$$H = \frac{d\sigma}{d\varepsilon_p} = \frac{E_T}{1 - E_T/E} \tag{19}$$

where E_T is elasto-plastic tangent modulus.

During the application of an incremental load, a node or particle may yield. All the stress and strain quantities are monitored at each Gaussian integration point and therefore it can be determined whether or not plastic deformation has occurred at such points. For any load increment, it is necessary to determine what portion of material is elastic and which part plastic. The stress return-mapping method [16, 17, 18] is employed here to let the stress satisfy the yield condition. For instance, if in the i-th iteration, the equivalent stress calculated using the linear constitutive relation is larger than the yield stress, it will then be mapped to the yield surface by the return-mapping technique.

b) Solving procedure

There are some methods for solving nonlinear problems such as Newton-Raphson method, corrected Newton-Raphson method and Initial Stiffness method [16]. In these methods, the external force, stress or displacement is applied in several steps and iteration method is used to calculate all stress and strain components in each step. At each sub-step, the unbalanced forces are also calculated by comparing equivalent nodal forces with the applied loads. The equivalent nodal forces are of element r, $\left(f^e\right)^r$

$$\left(f^e\right)^r = \iint_s B^T \sigma^r ds \tag{20}$$

[B] is the matrix of shape function derivatives which relates the nodal displacements to the strain and σ is state of stress on the element. F_{ext} is computed by assembling the equivalent nodal forces on the whole problem domain. The convergence tolerance is calculated by:

$$Tol = \left\|F_{unb}\right\| \Big/ \left\|F_{ext}\right\| \tag{21}$$

If convergence tolerance is greater than the specified value (for example 0.01), the residual forces are minimized by correcting internal stress until the specified convergence tolerance (0.02 in this work) is satisfied.

A cloud of nodes is assumed in the problem domain. The nodes in the problem domain are selected as the active nodes (Fig. 5a for initial step and Figs. 5b, 5c for successive steps). The stiffness matrix is calculated for active nodes based on natural element method. Figure 6 shows active Gauss points distribution used in gauss integration for stiffness matrix calculation. After each iteration, the new profile is obtained by the new location of nodes and the nodes on the new profile are selected as the active nodes for the next step. Then, the next external force or displacement growth is applied. The solving algorithm is presented in Fig. 7 [16].

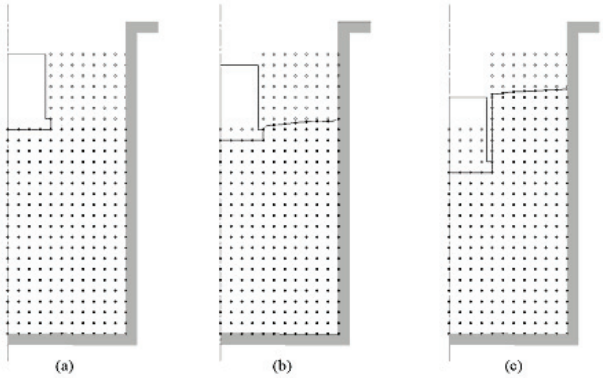

Fig. 5. Active node (solid circle) specification in different step of punch penetration

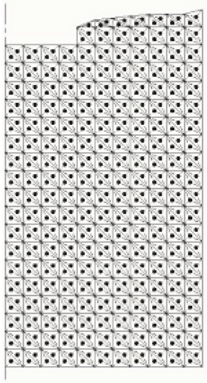

Fig. 6. Active Gauss points distribution for first step

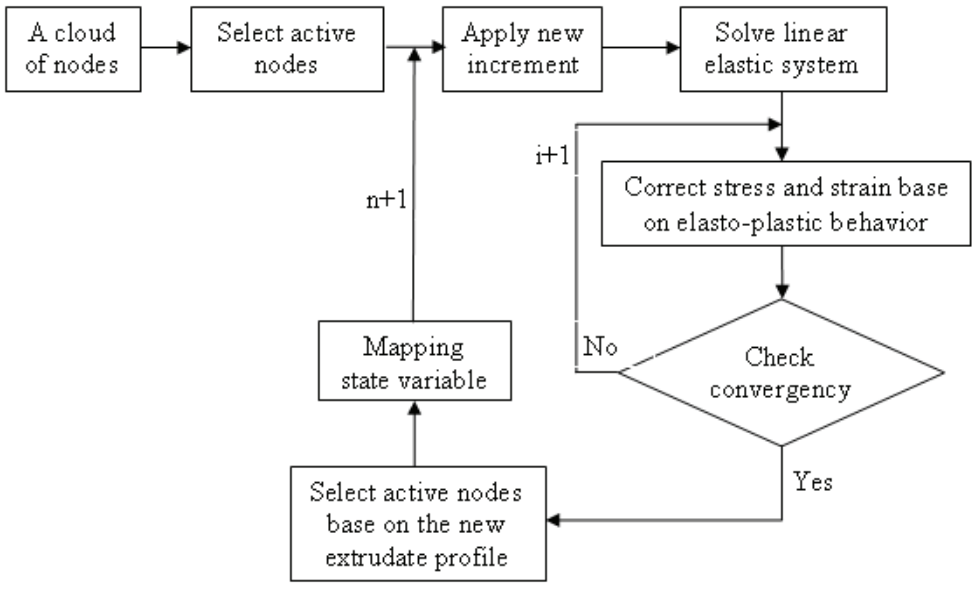

Fig. 7. Solving algorithm diagram

4. RESULTS AND DISCUSSION

A computer program based on NEM and re-meshed FEM calculations was developed and the validity and efficiency of the proposed NEM for two dimensional forming processes were evaluated by comparing the computer numerical results with those obtained from the experiment. Commercial aluminum was chosen as the work material for the experiments. Specimens made from round bars were annealed at 430° C for 3 hours. In order to obtain the material properties, compression tests were carried out at room temperature using a universal testing machine. From the tests, the stress-strain relationship was obtained as $\overline{\sigma} = 209\overline{\varepsilon}^{0.314}\ MPa$.

a) Simple tension test

In order to check the validity of NEM formulation, a simple uniaxial tension test was simulated and the result are compared to re-meshed FEM and well known Hollman-Ludwik law. In simple tension test, the stage before necking is homogeneous, whereas $\sigma = 209\overline{\varepsilon}^{0.314}\ MPa$ represents the stress-strain relationship for using material. The applied axial stress σ_{zz}, coincides with the flow stress $\overline{\sigma}$ for the load path, and the axial natural strain ε_{zz} is that of effective strain $\overline{\varepsilon}$.

$$\sigma_{zz} = \overline{\sigma} = \frac{F}{A},\quad \varepsilon_{zz} = \overline{\varepsilon} = \ln\frac{l}{l_0} \tag{22}$$

where l, l_0 are the current and original gage, respectively. Thus

$$\sigma = 209\varepsilon^{0.314} \rightarrow \sigma_{zz} = 209{\varepsilon_{zz}}^{0.314} \rightarrow \frac{F}{A} = 209(\ln\frac{l}{l_0})^{0.314} \rightarrow F = 209A\left[\ln\left(1+\frac{\Delta l}{l_0}\right)\right]^{0.314} \tag{23}$$

Considering no volume change:

$$A = A_0 l_0 / (l_0 + \Delta l) \tag{24}$$

Figure 8 shows the dimension of the tensile test specimen. Due to symmetry, only a quarter part of the specimen was used in the FE and NE simulation (Figs. 9, 10). The mesh agreement for FE simulation consists of 48 nodes and 66 triangle elements and for NE only 48 nodes are assumed for simulation. 10*mm* tensile displacement was applied in 150 sub-steps for the test loading. Figure 11 compares the force-displacement diagram obtained from the NE with FE and Hollman-Ludwik law. As it can be seen, very good agreement is achieved. Figure 12 compares the force-displacement diagram obtained from the NEM for different sub-steps (50, 75, 100, 150 and 200) with Hollman-Ludwik law. According to this figure, 100 sub-steps have the best agreement with Hollman-Ludwik law. Figure 13 compares the force-displacement diagram obtained from the NEM for several node distributions (21, 30, 36, 44 and 48) with Hollman-Ludwik law. It can be seen that the accuracy of the results increases as the number of nodes increases. Moreover, the diagrams for 36, 44 and 48 nodes are very close to each other and are in good agreement with Hollman-Ludwik law.

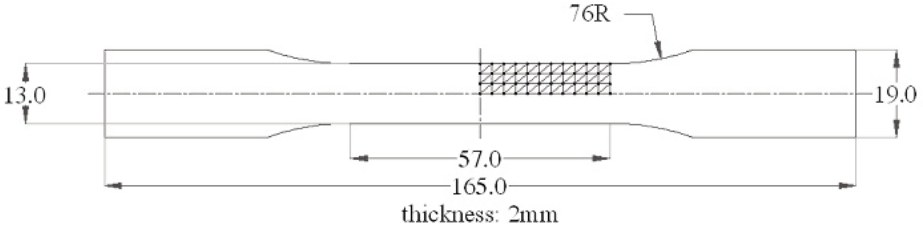

Fig. 8. Geometry of the tensile test specimen, (*mm*)

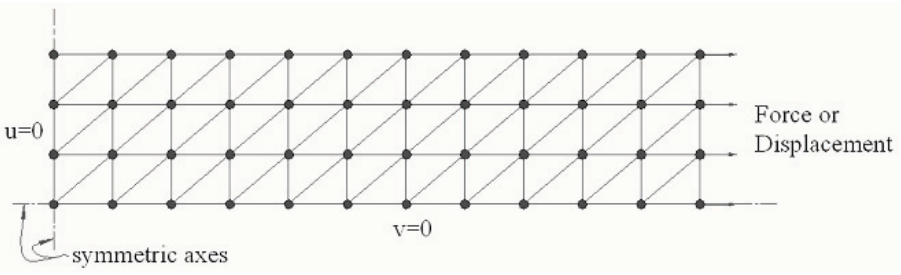

Fig. 9. Initial elements and nodes of a quarter of the tensile test

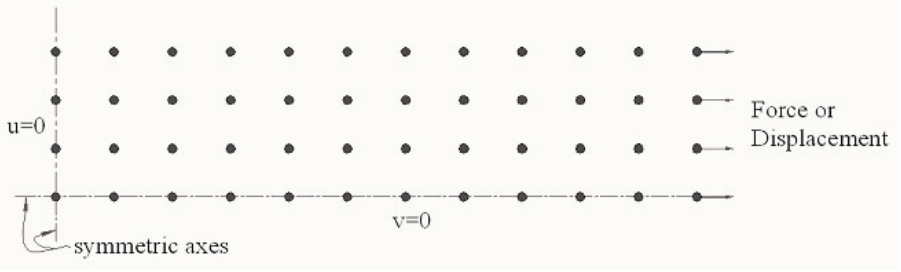

Fig. 10. Initial nodes distribution of a quarter of the tensile test

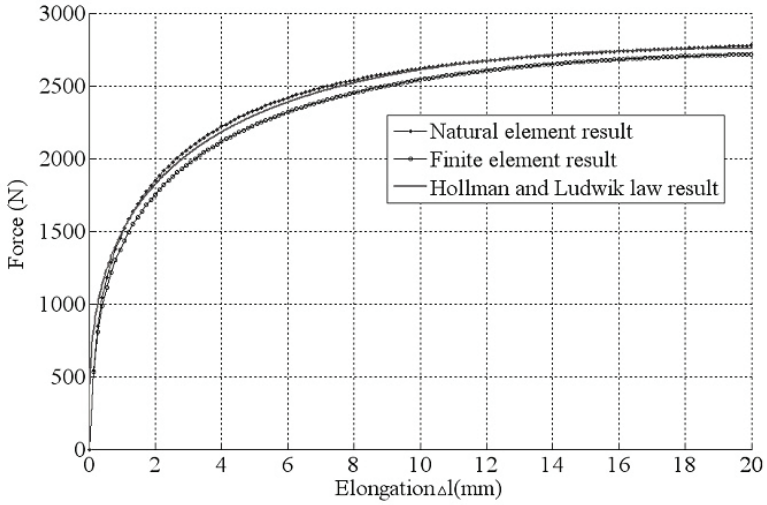

Fig. 11. Compression between Hollman-Ludwik law, FE and NE simulation results in tensile test

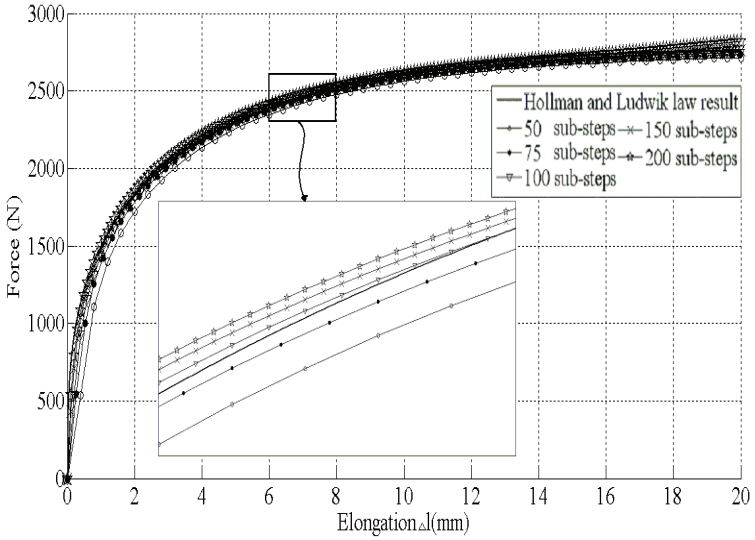

Fig. 12. Compression between Hollman-Ludwik law and several sub-steps in NE simulation results in tensile test

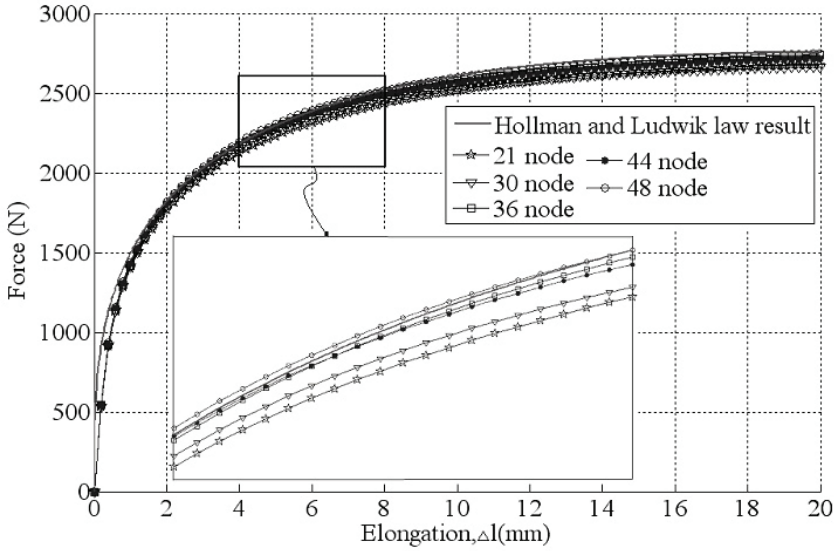

Fig. 13. Compression between Hollman-Ludwik law and several node distribution in NE simulation results in tensile test

b) Backward extrusion

Compression tests on flat, ring-shaped specimens were carried out to evaluate friction factor m. These tests exhibited values of the friction factor m between *0.15* to *0.22* depending on the type of lubricant. The friction factor at the die work-piece contact interface was estimated as *m=0.2*. Some work-pieces were cut into halves before extrusion and a square grid was printed on the contacting surface in order to be able to visualize the material flow. In order to maintain a close fit in the container two dumped and indented billets were used to produce the two halves for each backward extrusion billet. The tests were performed at room temperature with a slow strain rate. Circular-shaped tubes were produced from cylindrical-shaped billets and cylindrical punches.

A 200KN press and a proper constructed die set were used to perform the experimental tests [4, 5]. The extrusion loads were recorded during the experiments.

A 3D cylindrical billet is extruded through a rigid circular die as shown in Fig. 14. The punches dimensions and corresponding area reductions are given in Table 2. Backward extrusion is achieved by prescribing displacements at the top end of the punch. Due to Axial axisymmetry, only one half of 2D pattern is modeled. Figures 15 to 18 compare the NEM strain contour curves to those of the FEM results and experimental flow patterns. The simulation results truly indicate the formation of dead metal zone regions under the flat surface of the punches. These figures show NEM results are in agreement with the geometries observed from FEM and the experimental results. Also, the highly deformed region extending from the punch corner is clearly shown in both the NEM strain contour curves by comparison with the FEM strain contour curves and experimental grid distortions. Good agreement between the strain contours and experimental flow pattern are observed. In Figs. 19a to 19d, the comparison between the geometry profile for one quarter of the cross section of the extruded parts is presented. As can be seen, very good agreement is achieved. In Figs. 20a to 20d, the prediction forces from NEM simulation are compared with those of FEM simulation and the true forces obtained by experimental tests. The tolerance of workpiece, die and punch and the friction factor used in NEM simulation may be considered as error sources in the NEM simulation. The curves obtained from NEM simulation show a high increase in the forming force at the end of punch depression where the deformation zones collide at the bottom surface of the dies. The tendency of the curves shows good agreement between the NEM, FEM and the experiments.

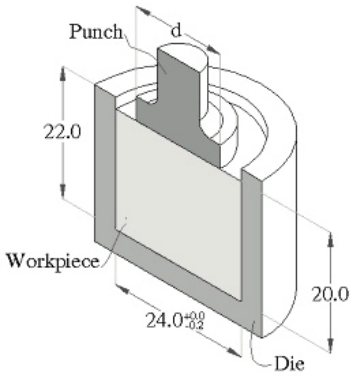

Fig. 14. Geometry of die, workpiece and punch, measurements in *mm*

Table 2. Punch diameter and reduction in area

d(*mm*)	10	12	14	16
Reduction in area	17.4%	25%	34%	44.4%

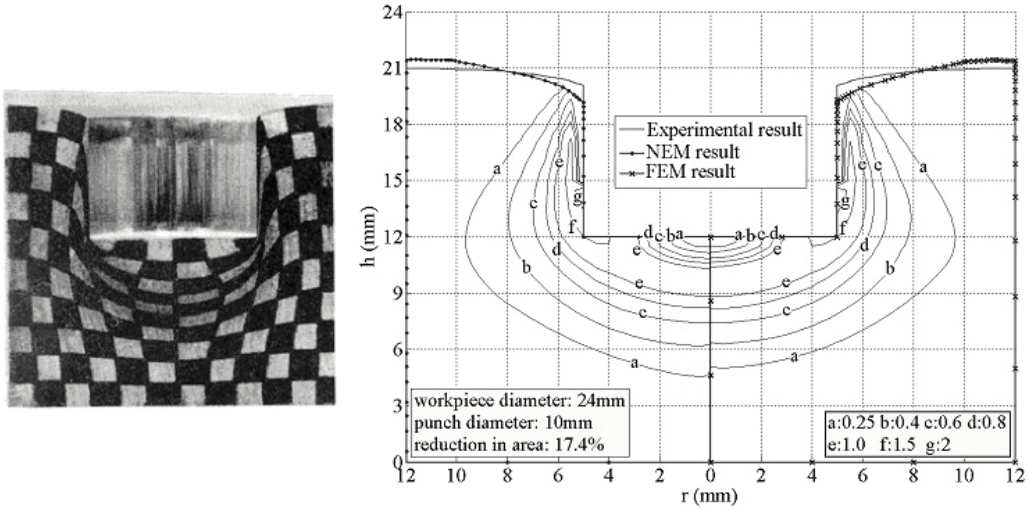

Fig. 15. Comparison between equivalent strain contour for 17.4% reduction in area

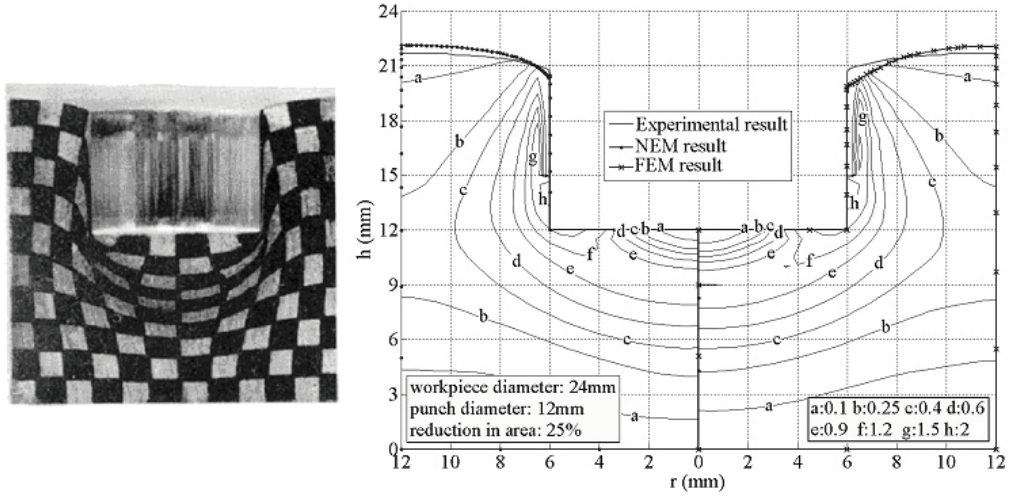

Fig. 16. Comparison between equivalent strain contour for 25% reduction in area

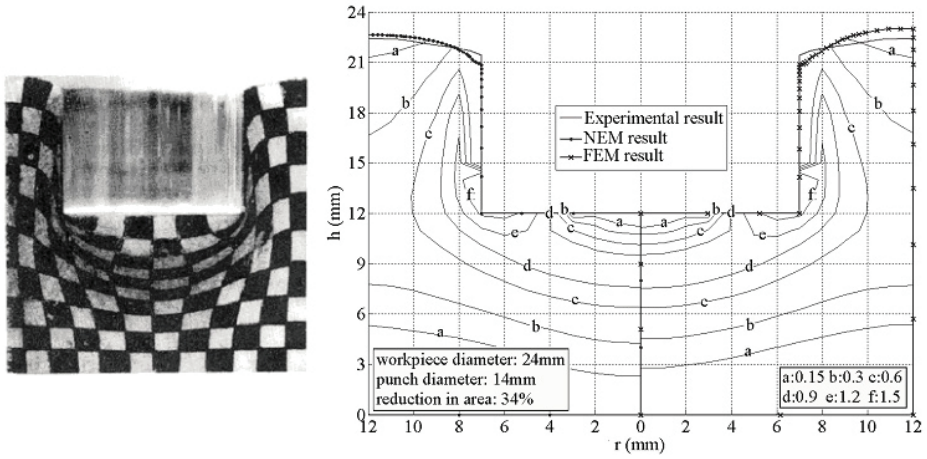

Fig. 17. Comparison between equivalent strain contour for 34% reduction in area

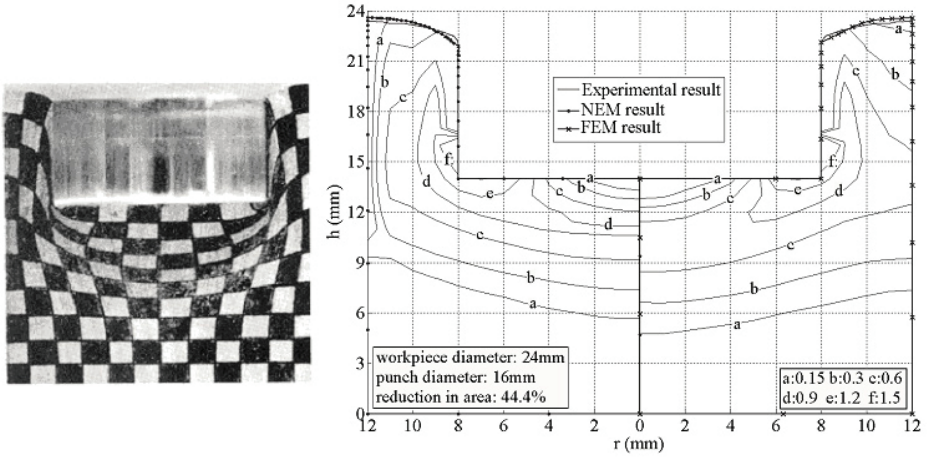

Fig. 18. Comparison between equivalent strain contour for 44.4% reduction in area

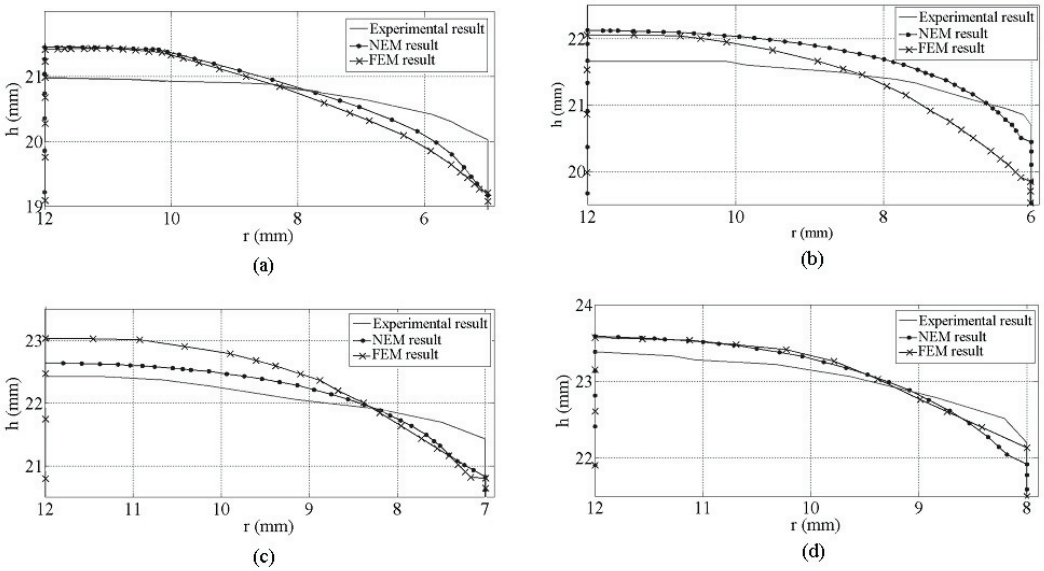

Fig. 19. Comparison between Geometrical profile for: a) 17.4% reduction in area b) 25% reduction in area, c) 34% reduction in area, d) 44.4% reduction in area

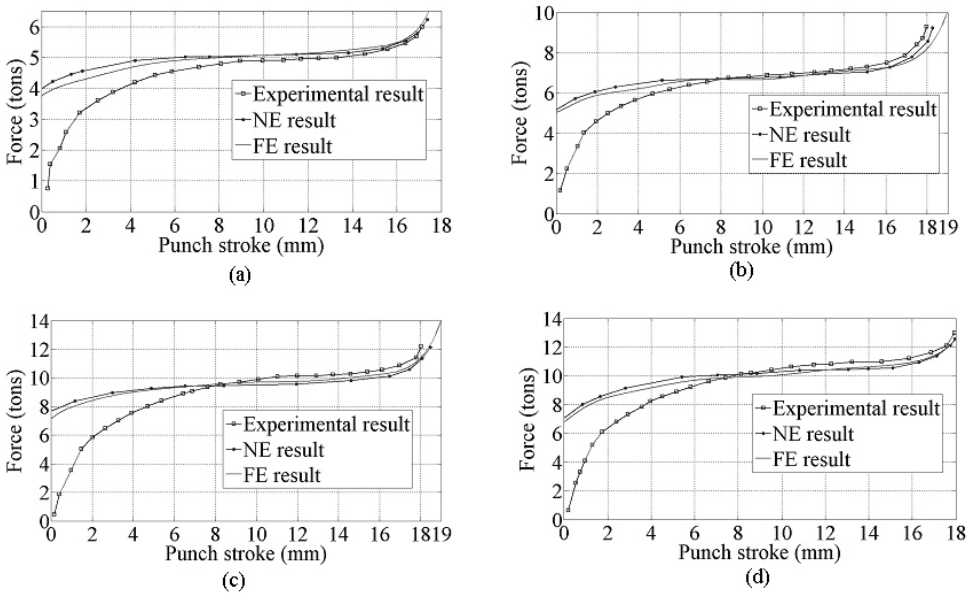

Fig. 20. Force-punch stroke diagram for: a) 17.4% reduction in area b) 25% reduction in area, c) 34% reduction in area, d) 44.4% reduction in area

5. CONCLUSION

A fundamental description of the natural element method and incremental plastic strain for solving non steady state metal forming problems like backward extrusion was examined. Experiments were also designed to cover the material flow, equivalent strain contour, geometry and forming load that are commonly found in axisymmetric backward extrusion. Commercial pure aluminum was used as testing material. The predicted forces obtained by NEM agree well with those obtained from FEM, and experiments and strain contour curves from simulation show dead metal zone regions under the flat surface of the punch. Identical results are observed from experimental grid distortion. The highly deformed region extending from the punch corner is observed in both simulation and experiments. This shows that the material around the punch corner rotates around the corner towards the punch side. Good agreement between NEM predictions, FEM results and experiments confirms the usefulness of the new approach for simulation of two-dimensional non-steady metal forming processes like backward extrusion.

REFERENCES

1. Marcal, P. V. & King, I. P. (1967). Elasto-plastic analysis of two-dimensional stress systems by the finite element method. *International Journal of Mechanical Sciences*, Vol. 9, pp. 143-155.
2. McMeeking, R. & Rice, J. R. (1975). Finite element formulation for problems of large elasto plastic Deformation. *Journal of International of Solids and Structures*, Vol. 11, pp. 601- 616.
3. Gouveia, B. P. P. A., Rodrigues, J. M. C. & Martins, P. A. F. (1998), Finite element modelling of cold forward extrusion using updated Lagrangian and combined Eulerian–Lagrangian formulations. *Journal of Materials Processing Technology*, Vol. 80–81, 647–652.
4. Moshksar, M. M. & Ebrahimi, R. (1998). An analytical approach for backward-extrusion forging of regular polygonal hollow components. *International Journal of Mechanical Sciences*, Vol. 40, No. 12, pp. 1247-1263.
5. Moshksar, M. M. & Ebrahimi, R. (1999). A new upper bound analysis for prediction of load and flow pattern in backward extrusion forging. *Iranian Journal of Science and Technology,* Vol. 23, No. 3, pp. 251-266.

6. Guo, Y. M. & Nakanishi, K. (2003). A backward extrusion analysis by the rigid-plastic integralless-meshless method. *Journal of Material Processing Technology*, Vol. 140, No. 1-3, pp. 19-24.
7. Guan, Y., Ahao, G., Wu, X. & Lu, P. (2007). Massive metal forming process simulation based on rigid/visco plastic element free Galerkin method. *Journal of Material Processing Technology*, Vol. 187-188, pp. 412-416.
8. Liew, K. M., Ng, T. Y. & Wu, Y. C. (2002). Meshfree method for large deformation analysis-a reproducing kernel particle approach. *Engineering Structures*, Vol. 24, pp. 543-551.
9. Lu, H., Cheng, H. S., Cao, J. & Liu, W. K. (2005). Adaptive enrichment meshfree simulation and experiment on buckling and post-buckling analysis in sheet metal forming. *Computer Methods in Applied Mechanics and Engineering*, Vol. 194, pp. 2569-2590.
10. Alfaro, I., Bel, D., Cueto, E., Doblare, M. & Chinesta, F. (2006). Three-dimensional simulation of aluminum extrusion by the alpha-shape based natural element method. *Computer Methods in Applied Mechanics and Engineering*, Vol. 195, No. 33-36, pp. 4269-4286.
11. Li, C. S., Liu, X. H. & Wang, G. D. (2007). Ring Upsetting simulation by the meshless method of corrected smooth particle hydrodynamics. *Journal of Materials Processing Technology*, Vol. 183, pp. 425-431.
12. Stoker, H. C. (1999). Development of arbitrary lagrangian-eulerian method in non-linear solid mechanics, applications to forming processes. *PhD Thesis*, University of Twente.
13. Sibson, R. A. (1981). *A brief description of natural neighbor interpolation*. Interpreting Multivariate Data, Barnett V. (ed). Wiley, Chichester, pp. 21-36.
14. Watson, D. (1981). Computing the n-dimensional delaunay triangulation with application to voronoi polytopes. *Computer Journal*, Vol. 24, No. 2, pp. 162-172.
15. Sukumar, N., Moran, B. & Belytschko, T. (1998). The natural element method in solid mechanics. *International Journal for Numerical Methods in Engineering*, Vol. 43, No. 5, pp. 839-887.
16. Owen, D. R. J. & Hinton, E. (1980). *Finite element in plasticity: theory and Practice.* Swansea (UK), Pineridge Press Limited.
17. Gadala, M. S. & Wang, J. (2000). Computational implementation of stress integration in FE analysis of elasto-plastic large deformation problems. *Finite Elements in Analysis and Design*, Vol. 35, pp. 379-396.
18. Lee, S. W., Yoon, J. W. & Yang, D. Y. (1998). Stress integration algorithm for plane stress eleastoplasticity and its application to explicit finite element analysis of sheet metal forming processes. *Computers and Structures*. Vol. 66, pp. 301-311.